Heliyon 10 (2024) e29315

Contents lists available at ScienceDirect

Heliyon

journal homepage: www.cell.com/heliyon

Research article

Comparing the crystal structures and spectroscopic properties of a *p*-hydroxy styrylquinolinium dye with those of its *p*-dimethylamino analogue

Mina Todorova [a], Rüdiger W. Seidel [b,1], Mihaela Stoyanova [a], Tsonko M. Kolev [c], Rumyana Bakalska [a,*]

[a] Plovdiv University, Faculty of Chemistry, 24 Tzar Assen Str., 4000, Plovdiv, Bulgaria
[b] Ruhr-Universität Bochum, Lehrstuhl für Analytische Chemie, Universitätsstraße 150, 44801, Bochum, Germany
[c] Institute of Molecular Biology "R. Tsanev", Acad. G. Bonchev Str, bl. 21, 1113, Sofia, Bulgaria

ARTICLE INFO

Keywords:
Stilbazolium dye
Hirshfeld surface analysis
X-ray crystallography
Crystal structure
Reversal solvatochromism
BLA

ABSTRACT

Two previously synthesized styrylquinolinium dyes, namely (*E*)-1-butyl-4-(4-(dimethylamino) styryl)quinolinium iodide (**D36**) and (*E*)-1-butyl-4-(4-hydroxystyryl)quinolinium iodide (**D34**), were compared in terms of their properties by single-crystal X-ray diffraction (XRD), Hirshfeld surface analysis, Fourier transform Raman (FT-Raman), Fourier transform infrared (FT-IR), fluorescence, and ultraviolet–visible (UV–Vis) spectroscopy, and ^{1}H- and ^{13}C-NMR methods. Both dyes **D36** and **D34** crystallized in the triclinic and monoclinic systems in the centrosymmetric space groups *P*-1 and $P2_1/n$, respectively. The unit cell of **D36** contains two molecules of the dye, participating in weak intermolecular interactions, whereas that of **D34** contains four formula units. The phenolic hydroxy group of **D34** participates in the formation of a hydrogen bond with the iodide anion. The 4-styrylquinolinium moieties of the cationic dye molecules are nearly planar. The dihedral angle between the mean planes through the ten-membered quinolinium system and the benzene ring is 7.5° in **D36** and 5.9(1)° in **D34**. The structural parameters planarity and bond length alternation (BLA) are discussed, which are important for the evaluation of the first hyperpolarizability β at the molecular level, even in a centrosymmetric crystal. The UV–visible spectra of the dyes in 14 solvents of different polarities were investigated. The reversible solvatochromic behavior of the dyes is demonstrated experimentally and compared with known "binuclear dyes" by evaluating the Rezende model. Dye **D36** does not fluoresce, and **D34** has a very low emission in the solvents tested.

1. Introduction

The design and development of organic nonlinear optical (NLO) materials with macroscopic second-order optical nonlinearities are of great interest, because they can be used for imaging biological objects as well as signal processing devices, ultra-high-speed optical

* Corresponding author.
E-mail addresses: minatodorova@uni-plovdiv.bg (M. Todorova), ruediger.seidel@pharmazie.uni-halle.de (R.W. Seidel), stoyanovamihaela99@gmail.com (M. Stoyanova), tskolev@bio21.bas.bg (T.M. Kolev), bakalska@uni-plovdiv.net (R. Bakalska).
[1] Current address: Martin-Luther-Universität Halle-Wittenberg, Institut für Pharmazie, Wolfgang-Langenbeck-Str. 4, 06120 Halle (Saale), Germany.

https://doi.org/10.1016/j.heliyon.2024.e29315
Received 1 April 2024; Accepted 4 April 2024
Available online 10 April 2024

communication, data storage, optical limiters, logic circuit devices, and optical switches [1–4]. Krieg et al. examined **D34** and related dyes to **D36** (Fig. 1), but with *N*-methyl and *N*-propyl tails acting as peroxidase's fluorescent substrates for application in histochemistry [3,4]. Compounds containing electron-donating (D) and electron-accepting (A) groups on opposite sides of a π-conjugated linker are highly significant among organic functional materials. Because of its extreme structural flexibility and diversity, the organic stilbazolium cation is arguably the most utilized chromophore to date for the synthesis of novel NLO materials [5]. A dye synthesized by our group, *viz.* 4-[(*E*)-2-(4-hydroxynaphthalen-1-yl)ethenyl)]-1-ethyl quinolinium bromide, deposited on a thin layer, has already proven nonlinear optical properties. The nonlinear absorption coefficient β is $-(3.3 \pm 0.7) \times 10^{-7}$ m/W, and the third-order NLO coefficient $\chi^{(3)}$ is 6.5×10^{-20} m^2 V^{-2} [6]. The study of structure–property relationships helps to decode the origin of optical nonlinearity at the molecular level, suggesting strategies aimed at discovering new materials. A crystal of acceptable quality and dimensions is needed for device applications. By selecting an appropriate solvent to optimize the growth conditions, high-quality single crystals can be produced. However, a non-centrosymmetric arrangement in the crystal must be present to observe high values of second-order nonlinear susceptibilities. Unfortunately, ca. 78 % of organic materials form centrosymmetric crystals [7]. Not to be overlooked are the alternative approaches to arrange such charged chromophores in a non-centrosymmetric fashion, such as anion metathesis, integration into polar thin films (of the Langmuir-Blodgett type), and polymer matrices [8]. Tweaking the BLA properties of a molecule is one of the most recent NLO techniques for creating chromophores. The method that can determine if an arrangement in the crystal structure is centrosymmetric or non-centrosymmetric is X-ray structural analysis.

These literature results inspired us to search for stilbazolium dyes with non-centrosymmetric chromophore arrangements and large molecular hyperpolarizability. Whereas *N*, *N*-dialkyl substituted dyes [5] have many crystal structures solved, hydroxy substituted stilbazolium dyes are known to be more difficult to grow crystals suitable for XRD [9–12]. In this study, we have carried out structural and spectroscopic analyses of the *p*-hydroxy substituted dye **D34**, comparing it with the previously reported by our group structure of *p*-dimethylamino analogue **D36** [13], because both dyes have the same chromophore with an *N*-butyl tail but different electron-donating groups (Fig. 1).

2. Experimental

2.1. Materials and synthesis

The details of the synthesis and physical-chemical properties of the dyes **D34** and **D36** used in the present work are discussed in the literature [14–19]. Our modified synthetic procedures, physical constants, and full spectral characterization of the compounds can be found in the Supplementary data.

2.2. X-ray crystallography

Crystals of **D34** suitable for single-crystal X-diffraction were grown by the slow evaporation technique from methanol/2-propanol at room temperature. The X-ray intensity data were collected on an Oxford Diffraction Xcalibur2 diffractometer with a Sapphire2 CCD and graphite-monochromated Mo-K_α radiation, using CrysAlisPro [20]. A semi-empirical absorption correction based on multiple-scanned reflections was applied [21], using ABSPACK in CrysAlisPro. The crystal structure was solved by direct methods using SHELXS-97 [22] and refined with SHELXL-2019/3 [23]. Anisotropic displacement parameters were introduced for all non-hydrogen atoms. Hydrogen atoms were placed in geometrically calculated positions and refined with the appropriate riding model. Hirshfeld surface analysis was carried out with CrystalExplorer [24].

*Crystal data for **D34***: $C_{21}H_{22}INO$, $M_r = 431.29$, $T = 120(2)$ K, $\lambda = 0.71073$ Å, monoclinic, $P2_1/n$, $a = 10.4493(2)$ Å, $b = 9.0956(2)$ Å, $c = 19.7318(5)$ Å, $\beta = 101.796(2)^\circ$, $V = 1835.76(7)$ Å^3, $Z = 4$, $\rho = 1.561$ g cm^{-3}, $\mu = 1.751$ mm^{-1}, $F(000) = 864$, crystal size $= 0.53 \times 0.06 \times 0.06$ mm, θ range $= 3.00–28.76^\circ$, reflections collected/unique $= 32{,}498/4428$, $R_{int} = 0.0578$, data/restraints/parameters $= 4428/0/219$, $S = 1.059$, $R1$ $[I > 2\sigma(I)] = 0.0339$, w$R2$ (all data) $= 0.0667$, $\Delta\rho_{max}$, $\Delta\rho_{min} = 0.74$, -0.53 eÅ^{-3}.

2.3. Spectroscopic measurements

The infrared and Raman spectra were recorded between 4000 cm^{-1} and 50 cm^{-1} on a VERTEX 70 FT-spectrometer (Bruker Optics). 25 scans were performed for each spectrum with a resolution of 2 cm^{-1}. The Raman spectra of **D36** and **D34** were measured at laser output power of 15 mW and 200 mW, respectively. The UV–Vis spectra (1 cm quartz cell and concentration range within 1×10^{-5} M were recorded on Agilent Cary 60 UV/Vis spectrometer operating between 190 and 800 nm, using solvents spectroscopic quality

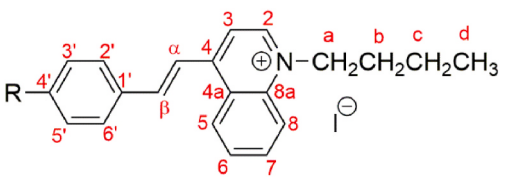

Fig. 1. Structural formula of the dyes **D34** (R═OH) and **D36** (R = NMe_2) showing the atom numbering used in the NMR assignments.

(Uvasol, Merck products). The maximum absorbance values of the dye obey the Bouguet-Beer-Lambert law as they were recorded at a concentration of the order of 10^{-5} M. UV–Vis spectra are normalized to the highest wavelength value of each spectrum. The fluorescence measurements were performed between 300 and 900 nm on PerkinElmer LS 45 fluorescent spectrometer in the same solvents at concentration 1×10^{-5} M and 10 nm slit. ^{1}H and ^{13}C-NMR measurements, referenced to TMS ($\delta = 0$ ppm), were made with Bruker Avance (500 MHz) spectrometer. The dyes were dissolved in DMSO-d_6.

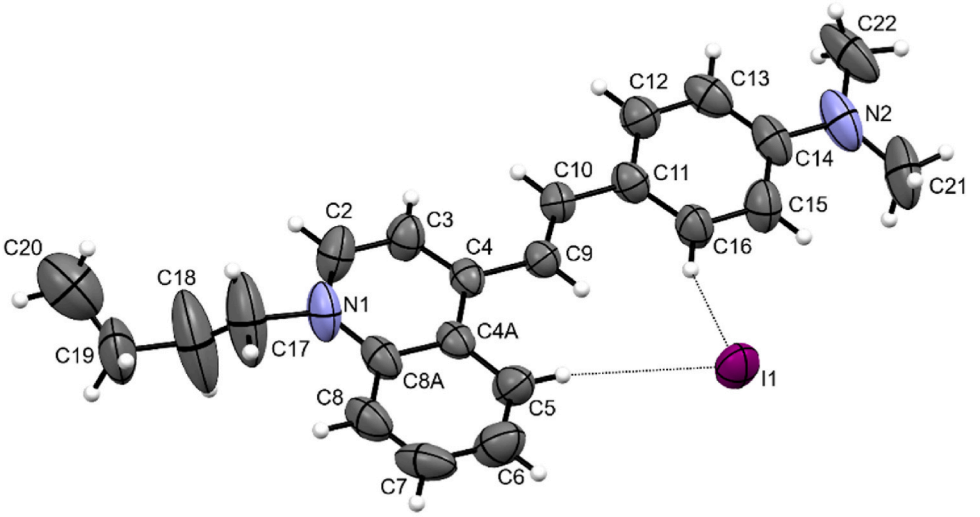

D36

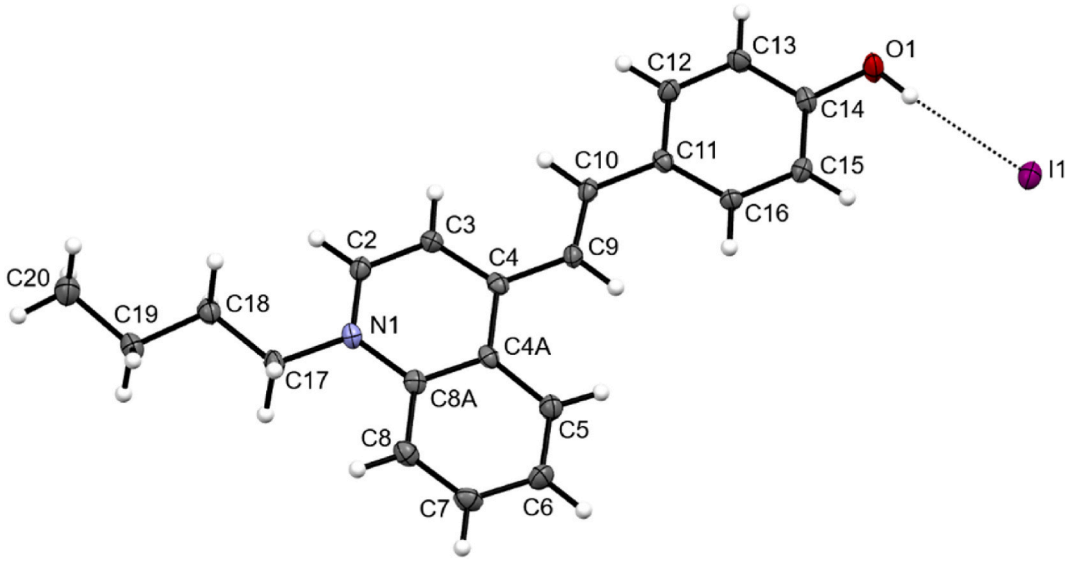

D34

Fig. 2. Molecular structures of **D36** (CSD refcode: ZEMDUT) and **D34** in the solid-state. Displacement ellipsoids are drawn at the 50 % probability level. Hydrogen atoms are represented by small spheres of arbitrary radius. Dashed lines illustrate C–H···I short contacts in **D36** and an O–H···I hydrogen bond in **D34**.

3. Results and discussion

3.1. Comparison of the solid-state structures of *D34* and *D36*

We have structurally characterized **D34** by X-ray crystallography, while a crystal structure determination for **D36** has previously been published in the Cambridge Structural Database (CSD) [25] with the CSD refcode ZEMDUT [13]. **D36** and **D34** crystallize in the centrosymmetric space group *P*-1 and $P2_1/n$, respectively. Fig. 2 shows the molecular structures in the solid-state, and Table 1 compares selected bond lengths and angles.

As expected, the configuration of the styryl C═C double bond is *E* in both **D36** and **D34**. The C4–C9═C10–C11 torsion angle is 178.6° in **D36** and 178.5(3)° in **D34**. The 4-styrylquinolinium moieties of the cationic dye molecules are nearly planar. The dihedral angle between the mean planes through the ten-membered quinolinium system and the benzene ring is 7.5° in **D36** and 5.9(1)° in **D34**. The most likely cause of the deviation from planarity are the contacts formed between the cations of the dye. In the centrosymmetric stacks of the dye cations one above the other, a slip is observed in which the benzene part of one molecule is located over the butyl tail of the antiparallel molecule and the quinolinium ring over the bridging double bond (Fig. 3). The corresponding stacking distances between the mean planes through the non-hydrogen atoms of the 4-styrylquinolinium moieties is 3.44 Å in **D36** and 3.34 Å in **D34**. Apart from face-to-face π···π stacking of the cationic dye molecules, C–H···I interactions in **D36** and an O–H···I hydrogen bond [$d(D\cdots A)$ = 3.417(2) Å] formed by the phenolic hydroxy group are the dominant intermolecular interactions in the solid-state. The overall crystal packing in **D36** and **D34** is distinctly different, despite the similar face-to-face π···π stacking in both structures (Fig. 4). In the triclinic crystal structure of **D36**, the dye molecules pack in a brick wall-like pattern. In contrast, the arrangement dye molecules in the monoclinic structure of **D34** may be described as a herringbone pattern.

To shed light on the crystal packing environments of the cationic dye molecules in the solid-state structures of **D36** and **D34** as a whole, we generated and visualized the Hirshfeld surfaces [26]. Fig. 5 shows the normalized contact distance (d_{norm}) mapped onto the Hirshfeld surface for **D36** and **D34** and the associated 2D fingerprint plots based on both contact distances between the nearest atoms

Table 1
Selected bond lengths and angles for **D36** (CSD refcode: ZEMDUT) and **D34**.

	D36	D34
C2–N1	1.328(8)	1.330(3)
C2–C3	1.377(8)	1.385(4)
C3–C4	1.378(7)	1.387(4)
C4–C4A	1.438(7)	1.434(4)
C4–C9	1.466(6)	1.452(4)
C4A−C8A	1.434(7)	1.419(4)
C8A−N1	1.375(8)	1.393(3)
C9–C10	1.326(7)	1.334(4)
C10–C11	1.448(7)	1.453(4)
C11–C12	1.395(7)	1.399(4)
C11–C16	1.402(7)	1.405(4)
C12–C13	1.378(7)	1.381(4)
C13–C14	1.401(9)	1.390(4)
C14–C15	1.386(9)	1.395(4)
C14–N2	1.386(7)	–
C14–O1	–	1.355(3)
C15–C16	1.389(7)	1.379(4)
C17–N1	1.511(8)	1.495(3)
N1–C2–C3	122.2(6)	122.6(2)
C2–C3–C4	120.9(6)	121.1(3)
C3–C4–C4A	117.8(4)	116.7(2)
C3–C4–C9	121.9(5)	122.5(2)
C4A−C4–C9	120.3(4)	120.8(2)
N1–C8A−C4A	118.7(5)	118.9(2)
C2–N1–C8A	121.3(5)	120.2(2)
C8A−C4A−C4	119.0(5)	120.4(2)
C10–C9–C4	124.3(5)	125.8(2)
C9–C10–C11	126.5(5)	126.6(2)
C12–C11–C16	116.6(5)	117.3(2)
C12–C11–C10	120.3(5)	119.7(2)
C16–C11–C10	123.1(5)	123.0(2)
C13–C12–C11	122.1(6)	121.9(2)
C12–C13–C14	121.1(6)	119.8(3)
C13–C14–C15	117.4(5)	119.6(2)
C16–C15–C14	121.4(6)	120.1(2)
C15–C16–C11	121.4(5)	121.4(2)
N2–C14–C13	122.1(6)	–
N2–C14–C15	120.5(6)	–
O1–C14–C13	–	117.6(2)
O1–C14–C15	–	122.8(2)

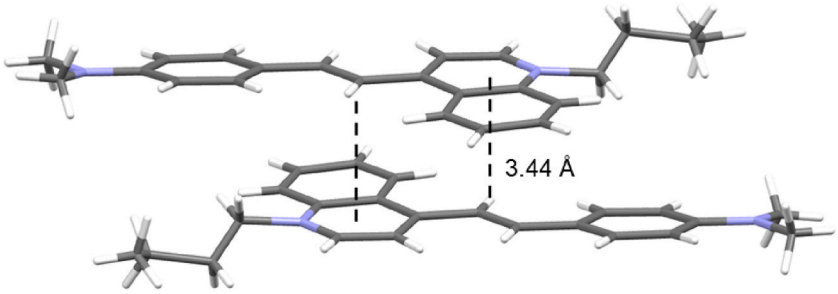

D36

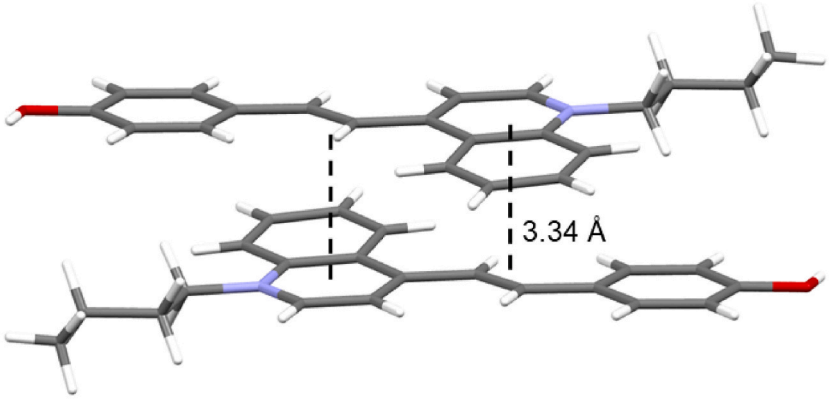

D34

Fig. 3. Centrosymmetric antiparallel stacks of the cationic chromophores in the crystal structures of **D36** (CSD refcode: ZEMDUT) and **D34**. Color scheme: C, grey; H, white; N, blue; O, red. (For interpretation of the references to color in this figure legend, the reader is referred to the Web version of this article.)

inside (d_i) and outside (d_e) the surface. Apart from the classical O–H···I hydrogen bond, which is only present in **D34**, the Hirshfeld surface analysis reveals the similarity of the intermolecular interaction patterns in **D36** and **D34** in spite of the markedly different crystal packing of the compounds.

BLA (bond length alternation) and planarity are the main structural factors that are crucial for estimating the first hyperpolarizability at the molecular level, even in a centrosymmetric crystal [27,28]. The planar configuration favours π-conjugation and hence polarization in the D-π-A molecules, resulting in the appearance of a dipole moment, and this has a positive impact on the value of the first hyperpolarizability β [29]. A measure of the degree of polarization in a conjugated system, the structure parameter BLA is defined as the average difference between the lengths of neighbouring single (C–C) and double (C═C) bonds [30]. The best value of BLA, at which maximum values of the first hyperpolarizability are produced, is 0.1 Å. Substances having a BLA value of zero were discovered to exhibit no nonlinear optical activity [31]. The calculated BLA parameter values for the dyes **D36** and **D34** are 0.067 and 0.117 Å, respectively. The two aromatic fragments' deviations from the bridge system's plane above 3° provide the most likely reason for the deviations from the optimal value of the BLA parameter.

3.2. UV–Vis and fluorescence spectroscopic study

The substances being studied are salts that are soluble in polar organic solvents but just a little in nonpolar ones. The specific interaction in the solution, which involves a formation of hydrogen bonds and charge transfer complexes, may alter the HOMO-LUMO energy difference, leading to a shift in the equilibrium-excited state level to a higher/lower energy in the polar solvent. Fig. 6 shows a schematic illustration of the excited and ground states of two chromophores. The positive charge of the chromophore is localized on a different type of heteroatom in each of the different forms because it moves from the pyridinium moiety to the amino/OH group upon excitation. In the ground state (a), it is on the quinolinium nitrogen, and in the excited state (b), it is on the imine nitrogen or oxygen. It is significant to observe that the charge can be delocalized more effectively in the benzoid form (a) than in the quinoid form (b), due to

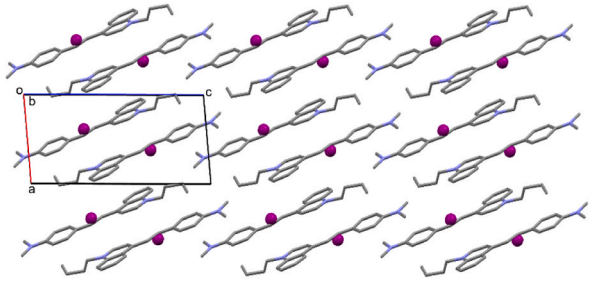

D36

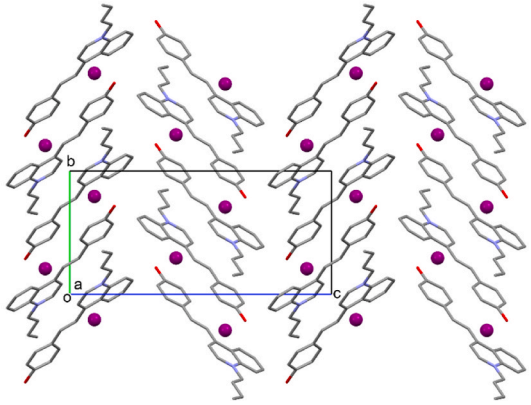

D34

Fig. 4. Packing diagrams of **D36** and **D34**, viewed along the *b* and the *a* axis respectively. Color scheme: C, grey; I, purple; N, blue; O, red. Hydrogen atoms are omitted for clarity. (For interpretation of the references to color in this figure legend, the reader is referred to the Web version of this article.)

deviation from planarity of the two parts of the latter. As a result, solvents can interact with both forms in various manners based on their polarity, as shown on Fig. 6 with alcohol as an example.

Taking into account the solubility of dyes and the characteristics of solvents, 14 solvents with different proton donor (HBD = H-bond donor) and proton acceptor (HBA = H-bond acceptor) abilities were selected [32]. The hydroxyl solvents water, methanol, ethanol and n-butanol were selected as HBD (E_T^N 0.5 ÷ 1), and dipolar aprotic solvents (E_T^N 0.3 ÷ 0.5) were acetonitrile (MeCN), dimethylsulfoxide (DMSO), dimethylformamide (DMF), acetone, 1,2-dichloroethane (DCE), pyridine, and non-polar HBA (E_T^N 0 ÷ 0.3) - chloroform, ethyl acetate, tetrahydrofuran (THF) and 1,4-dioxane. In the last four solvents, the dye **D34** is insoluble. Normalized UV–Vis spectra of the dyes are shown in Fig. 7, and Table 2 presents the experimental data together with the relevant polarity values for the mentioned solvents.

While the Vis spectrum of **D34** has two to three absorbance bands in nearly all of the examined solvents, the dye **D36** only has one maximum in the visible region around 550 nm, which belongs to the CT band. The CT band of the quinoid form (QF) of **D34** dye is located in the longer wavelengths between 607 and 676 nm, while the CT band of the benzoid form (BF) is located in the shorter wavelengths between 415 and 470 nm. Aggregation frequently results in the splitting of the quinoid form's long-wavelength absorption band (Fig. 7b). The monomer of the quinoid form is liable for the longest band, and the dimer is responsible for the shorter band at around 620 nm, which is frequently just hinted at as a shoulder. Depending on their polarity, the solvents can stabilize both the BF and QF forms in different way. Because of this, it is possible that just the benzoid form or the quinoid form was present in some solvents while both forms were present in others. The analysis shows that in the group of HBD solvents, the dye **D34** has a similar behaviour – in aqueous solutions, it exists only in its BF, but in alcohol solutions both forms were present. Both forms were also present in aprotic solvents. Dyes of this kind are very sensitive to traces of moisture or acids in the solvents tested.

The difference in maximum values observed in 1,2-dichloroethane and water solvents, or the **D36** shift, is 75 nm (133 cm^{-1}) (Fig. 7a). However, the CT band shift from water to chloroform is 43 nm, which is almost twice as small as the same solvent shift of the "binuclear" DANSQI dye (84 nm) [33]. The spectral shift of the absorption maximum due to the changing solvent polarity is 262 nm for the phenolic dye **D34**.

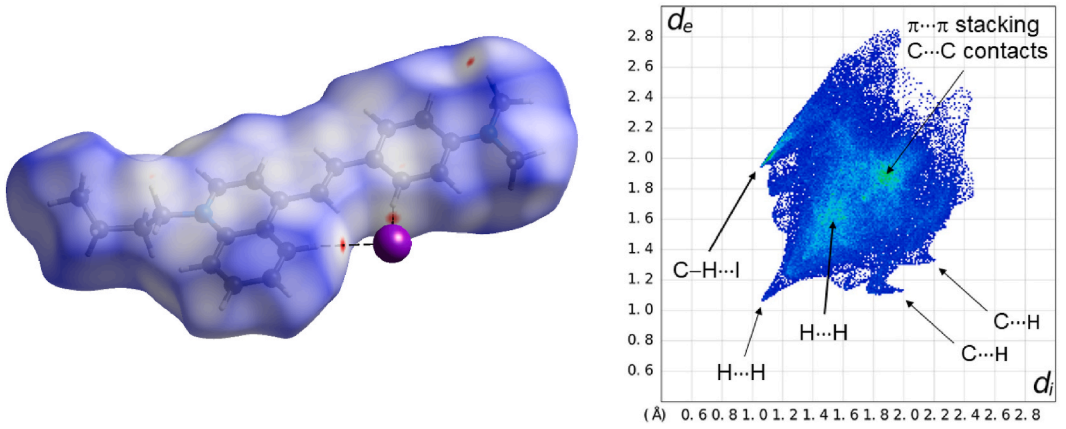

Fig. 5. Hirshfeld surfaces for **D36** and **D34** mapped with d_{norm} (red areas indicate short contacts) and the corresponding 2D fingerprint plots d_e versus d_i. Color scheme for the atoms: C, grey; H, white; I, purple; N, blue; O, red. (For interpretation of the references to color in this figure legend, the reader is referred to the Web version of this article.)

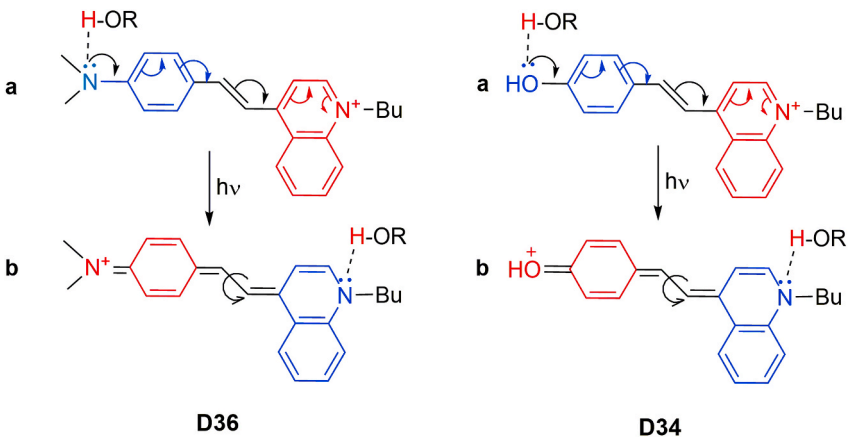

Fig. 6. Schematic representation of the ground state a) benzoid (BF) form; and b) the excited state quinoid (QF) form of the chromophores and the solvatation of HBD-molecule, for example. In the diagram, the donor part is in blue and the acceptor is in red color. (For interpretation of the references to color in this figure legend, the reader is referred to the Web version of this article.)

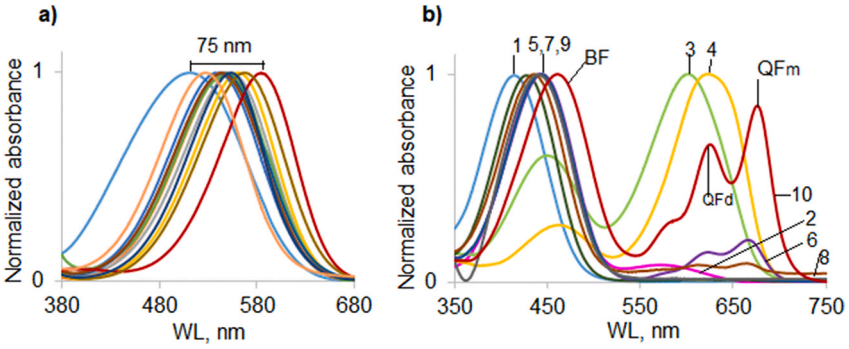

Fig. 7. Normalized UV–Vis spectra of the dyes a) **D36** and b) **D34** in different polarity solvents. The **D36** shift between water and 1,2-dichloroethane is 75 nm (a). The numbers of the spectra correspond to the numbers of the solvents in Table 2. The designation BF is the abbreviation of benzoid form; QFm is quinoid form (monomer); QFd is quinoid form (dimer).

Table 2
Electronic properties of the dyes **D36** and **D34** in solvents of different polarity parameters.

N⁰	Solvent	E_T^N	D36		D34					
			Abs	E_T(D36)	Abs		Em	E_T(D34) BF	E_T(D34) QF(m)	Stokes shift[a]
					BF	QF(m/d/n)				
1.	water	1.000	512	55.90	414	–	554	68.98		140
2.	methanol	0.762	548	52.13	442	580 br	552	64.69	49.30	110
3.	ethanol	0.654	553	51.66	453	607	564	63.12	47.06	103
4.	n-butanol	0.586	562	50.87	470	627	553	60.83	45.60	83
5.	MeCN	0.460	542	52.85	428	–	550	66.80	–	122
6.	DMSO	0.444	550	52.03	444	662/624	575	64.40	43.19	130
7.	DMF	0.386	545	52.41	443	–	560	64.54	–	117
8.	acetone	0.355	544	52.61	438	662/614/567	550	65.28	43.19	112
9.	DCE	0.309	586	48.79	434	–	533	65.80	–	99
10.	pyridine	0.302	568	50.29	461	676/624/584	n.a.	62.02	42.30	–
11.	chloroform	0.259	554	51.56		–	–		–	
12.	ethylacetate	0.228	537	53.24	–	–	–	–	–	
13.	THF	0.207	541	52.85	–	–	–	–	–	
14.	1,4-dioxane	0.164	529	54.05	–	–	–	–	–	

Abbreviations: E_T^N is the normalized value of a molar transition energy and for the reported solvents were taken from Ref. [32]; Abs is λ_{max} (A) (nm) of CT band; Em is λ_{max} (Fl) (nm); E_T(D36) and E_T(D34) are corresponding intramolecular transfer energy of charge of **D36** and **D34** in kcal.mol^{-1}; BF is benzoide form; QF (m/d/n) is quinoid form (monomer/dimer/n-mer); br is a broad band; n.a.- not available.

[a] Stokes shift is the difference in nanometers between positions of the band maxima of the absorption and emission spectra.

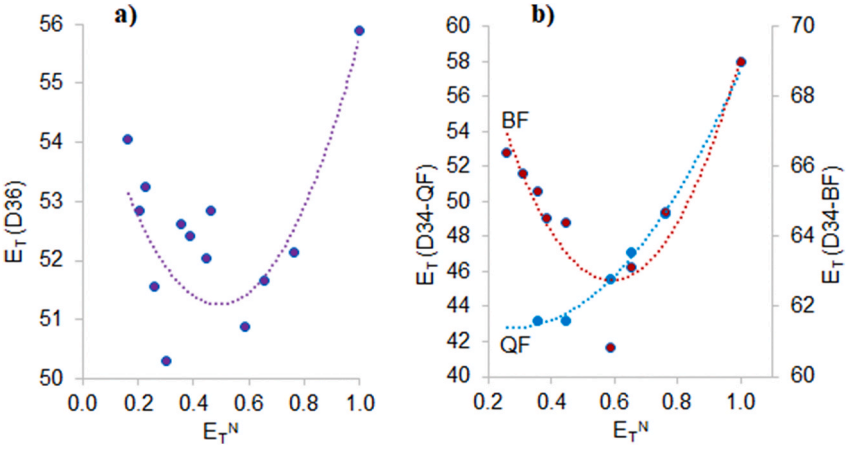

Fig. 8. Plots of the dependence a) of E_T (D36) and b) of E_T (D34) in its BF and QF vs. E_T^N of solvents of different polarity. E_T (dyes) is given in units of kcal mol^{-1}.

What is the sign of the solvatochromism of the dyes under study? In 2010, Domínguez and Rezende linked the chemical hardness (η) of a molecule to its charge distribution, creating a generalized model to predict the solvatochromic behaviour of cyanines [34,35]. We calculated the chemical hardness η for the dye chromophore **D36**, using the data from the published tables [34], as a sum of the hardness of the fragments: 104.6 kcal mol^{-1} for the donor fragment $\mathbf{d_1}$, 85.4 kcal mol^{-1} for the acceptor fragment **a17** and 5 kcal mol^{-1} for the amino group, $\eta = 104.6 + 85.4 + 5 = 195.0$ kcal mol^{-1}. For **D34** the sum of the hardness of the fragments is: $\mathbf{d_1}$ + **a17**+ OH group, $\eta = 104.6 + 85.4 + 5.1 = 195.1$ kcal mol^{-1}. These values, according to the model of Domínguez and Rezende, predict a reversible solvatochromism.

Is this really the case? In order to clarify the solvatochromic behaviour of the dyes, we used the experimental data from the UV–Vis spectroscopic study to construct the graphical dependence of the transition energies of the dyes in different solvents against the E_T^N polarity parameter for the same solvents (Fig. 8). The corresponding intramolecular charge transfer energy E_T (dye) in kcal mol^{-1} (1 kcal mol^{-1} = 4.184 kJ mol^{-1}) was calculated according to equation (1) [32]:

$$\mathbf{E_T\ (Dye)} = \frac{\mathbf{28591.5}}{\lambda\ \mathbf{max}\ \mathbf{(nm)}} \tag{1}$$

The Rezende model represented the solvatochromic plots (Fig. 8) as a hyperbolic curve with a minimum of reversal. We may conclude that both dyes exhibit real reversible sovatochromic behavior based on experimental measurements in a sufficiently broad range of solvents.

From the available experimental range of solvents, it can be said that the reversal of solvatochromism for dye **D36** occurs in solvent DMSO with a critical point of $E_T(30)$ value of 49.7 (E_T^N value 0.586). However, for dye **D34**, this event occurs in the solvent *n*-butanol, with a critical point of $E_T(30) = 45.1$ ($E_T^N = 0.444$).

It is well known that increasing the annelation of the donor or acceptor fragment has a significant impact on the dye's ground and excited states, making the former less zwitterionic and eventually switching its negative solvatochromism to reversed behavior [8,35]. Therefore, we make a comparison with the "binuclear" dimethylamino-substituted dyes reported earlier by our group [8,33]. Fig. 9 compares the CT band maxima of dyes **D36**, **D34,** and DANSQI [33] registered in a common list of solvents. The difference between DANSQI and **D36** comes down to the shift of λ_{max} of **D36** by about 50 nm to longer wavelengths (bathochromic shift), which means lower transition energies for "one and half nuclear" dye **D36**. Comparison between the hydroxy substituted dye **D34** and the dimethylamino substituted **D36** shows about 100 nm lower wavelengths for **D34**.

In Fig. 10, one can see the hyperbolic inversion minima curves of the three stilbazolium dyes for their total solvent ranges - DANSQI [33], 4-{(*E*)-2-[4-(dimethylamino)naphthalen-1-yl]ethenyl}-1-pentylquinolinium bromide dihydrate (**III**) [8] and **D36**. It is clear that all three dyes show reversed solvatochromic behaviour.

However, there appears to be a discrepancy with the Rezende model [34]. The problem is that by calculating the chemical hardness η of the chromophore of DANSQI and the dye 4-{(*E*)-2-[4-(dimethylamino)naphthalen-1-yl]ethenyl}-1-pentylquinolinium bromide dihydrate (III), which is common to both dyes, as a sum of the hardnesses of the donor fragment **d2**, the acceptor fragment **a17** and the amino group, we get $\eta = 85.4 + 83.6 + 5.0 = 174$, which value suggests positive solvatochromism. We experimentally proved that these dyes exhibit "true" reversed solvatochromic behaviour.

Both dyes under study were also investigated with respect to their emission properties in solvents of different polarities. Whereas **D34** exhibits weak fluorescence, **D36** shows no emission of its own. Fluorescence spectra were appended in the Supplementary data (Figs. S1–S5). The photoinduced processes model developed through in-depth experimental and theoretical studies can be used to

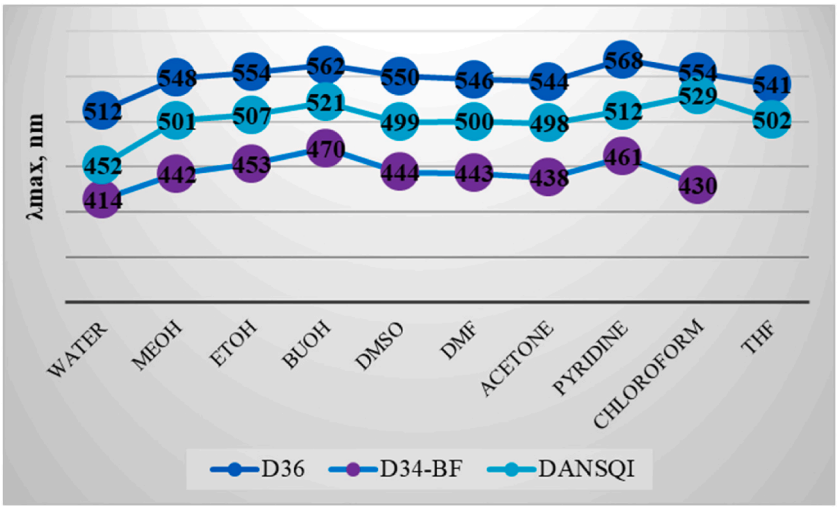

Fig. 9. Comparison between CT absorption band maxima in the spectra of dyes **D36**, **D34**, and DANSQI [33] measured in a common list of solvents: (1) water, (2) methanol, (3) ethanol, (4) *n*-butanol, (5) DMSO, (6) DMF, (7) acetone, (8) pyridine, (9) chloroform, and (10) tetrahydrofuran.

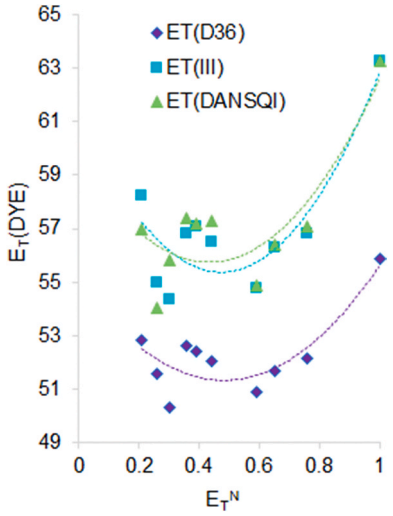

Fig. 10. Comparaison of Rezende model solvatochromic plots for the three stilbazolium dyes DANSQI [33], **III** [8], and **D36**.

evaluate the photophysical properties of **D36** and **D34** [36–39]. The model takes into account two possible deexcitation pathways. Following photoexcitation into the Franck-Condon (FC) state, the dye returns to the S_0 surface either through a twisted intramolecular charge transfer (TICT) state, which is dark, or through a partially relaxed "locally excited" (LE) state, which is a radiative process. By twisting the olefinic double bonds, this sort of conformer is created. The polarity and viscosity of the solvent are two environmental factors that heavily influence the rotating movements of the dye molecules. The dyes can be utilized for guest-host complexation for the fluorescence detection of non-fluorescent analytes due to these features [36].

3.3. *Infrared and Raman spectroscopic study*

The IR and Raman spectra of **D36** and **D34** in the solid state are appended in the Supplementary data (Figs. S6–S9). The spectral picture of the styrylquinolinium dyes in IR spectra is complicated and needs detailed study. Nearly all IR bands are asymmetric. The solid state effects, such as Davidov splitting, and Evans holes effects are observed [40]. Since the electron interaction between the strongest neutral donor and one of the strongest acceptors, the quinolinium fragment, leads to electronic interaction, which in turn results in a vibrational one, that is why nearly all vibrations are strongly mixed and the intensities are strongly influenced. This has been confirmed by the detailed interpretation of the IR spectrum using quantum chemical calculations of 4-{(*E*)-2-[4-(dimethylamino) naphthalene-1-yl]ethenyl}-1-methyl quinolinium iodide monohydrate (DANSQI) [33]. The vibrational spectra of **D36** were compared to the spectra of DANSQI. Table 3 presents characteristic band assignments from the vibrational spectra of **D36**.

The band at 1575 cm^{-1} in the IR spectrum and at 1576 cm^{-1} in the Raman spectrum is mixed vibration including ν ($C \doteq C$) of the two aromatic nuclei. The band at 1542 cm^{-1} belongs to δ^s synphase vibration of both CH_3 and the DMA group. The bands at 1436 cm^{-1} (IR) and 1433 cm^{-1} (Raman) are attributed to the mixed skeletal vibrations of the aromatic moieties with out-of-plane vibration $\gamma_{C\text{-}H}$ of the double bridge bond. The bands at 1377, 1332, 1301, 1292, 1226, 1191 cm^{-1}/1379, 1333, 1306, 1287, 1236, and 1190 cm^{-1} in both IR and Raman spectra are assigned to the mixed vibrations, which include in the plane deformation vibrations of aromatic skeletal, of the C–H groups of both rings and double bond, and the dimethylamino group. The bands for the deformation C–H vibrations of the methyl groups in the *N*,*N*-dimethylamino group (DMA) are observed at 1120 cm^{-1} (IR)/1123 cm^{-1} (Raman). Breathing vibrations of the aromatic nuclei were observed at 1047 cm^{-1} in the IR spectrum.

Most of the vibrations of DMA are mixed with the vibrations of other functional groups, as can be seen from Table 3. The deformation vibrations δ(C–H) of the methyl groups of DMA are observed at 941, 1226, and 1377 cm^{-1} in the IR spectrum and at 938, 1236, 1379, and 1494 cm^{-1} in the Raman spectrum. Several pure vibrations of the DMA group are also observed. An asymmetric deformation vibration δ^{as} (C–H) (DMA) is shown at 1542 cm^{-1} in both spectra. An asymmetric stretching vibration ν^{as} (C–H) (DMA) is observed at 3078 and 2955 cm^{-1} in the IR spectrum.

The bands in the IR and Raman spectra of compound **D34** were compared with those (theoretical and experimental) of a series of hydroxystyrylquinolinium dyes [41]. The assignment of the bands in the IR and Raman spectra of **D34** to the corresponding normal vibrations is presented in Table 4. The table shows that the bands are the result of mixed vibrations. The comparison of the IR and Raman spectra of **D34** with the experimental and theoretical spectra of a series of hydroxy dyes also shows complete agreement.

3.4. *^{1}H- and ^{13}C-NMR spectroscopic study*

The assignments of the multiple signals, especially those of the methine protons and carbon atoms in the NMR spectra of **D36** and **D34** was well confirmed by the homonuclear correlation spectroscopy (COSY), heteronuclear single-quantum correlation spectroscopy

Table 3
The measured IR and Raman frequencies and the assignment of the bands to the corresponding normal vibrations of the dye **D36**.

Observed IR Frequency [cm^{-1}]	Observed Raman Frequency [cm^{-1}]	Calculated IR Frequency [cm^{-1}] [33]	Vibrational Assignments
420	414	421	skel. def. ip
433		437	γ(C–H) aromatic nuclei
487		487	ring puckering NF, $\delta(C \doteq C)$ QF
501	500	501	mix vibr. δ ($C \doteq C$) aromatic nuclei
871	876	869	γ(C–H) aromatic nuclei
941	938	947	skel. vibr. aromatic nuclei + δ(DMA) + γ(C–H) QF
1120	1123	1129	δ(C–H) of the both CH_3 groups in DMA
1191	1190	1190	β(C–H) QF
1226	1236	1229	β(C–H) aromatic nuclei + δ(DMA)
1292	1287	1284	β(C–H) aromatic nuclei + β(C–H) (C]C)
1301	1306	1301	β(C–H) aromatic nuclei + β(C–H) (C═C)
1332	1333	1330	β(C–H) C]C + β(C–H) aromatic nuclei, ν(C–C) aromatic nuclei
1377	1379	1376	β(C)+ β(C–H) aromatic nuclei + β(CH) (C]C) + ν(C–N–C) + DMA
1436	1433		$\nu(C \doteq C)$ QF + $\nu(C \doteq C)$ aromatic nuclei + βC-H (C═C)
	1494	1492	$\nu(C \doteq C)$, β(C–H) aromatic nuclei + δ^{s} and δ^{as} CH_3 (DMA)
1542	1542	1550	δ^{as} (CH_3) (DMA)
1575	1576	1570	ν ($C \doteq C$)aromatic nuclei
2955	2954	2959	ν^{as} (CH_3) (DMA)
3078		3079	ν^{as} (CH_3) (DMA) synphase

Abbreviations: DMA (*N*-dimethylamino group), BF – benzene fragment, QF quinoline fragment, ν - stretching vibration, δ - deformation vibration, β - in plane deformation vibration, γ - out of plane vibration.

Table 4
The measured IR and Raman frequencies and the assignment of the bands to the corresponding normal vibrations of the dye **D34**.

Observed IR Frequency [cm^{-1}]	Observed Raman Frequency [cm^{-1}]	Calculated IR Frequency [cm^{-1}] [41]	Vibrational Assignments
428		431	ring puckering BF + γ(O–H)
466		466	skel. def. of aromatic nuclei + $\beta(C \doteq C)$aromatic nuclei
482	480	485	$\beta(C \doteq C)$aromatic nuclei
588		583	γC-H (C═C) + $\beta(C \doteq C)$aromatic nuclei + $\gamma(C \doteq C)$ aromatic nuclei
713		712	β ($C \doteq C$)aromatic nuclei
806		801	$\delta(C \doteq C)$aromatic nuclei + β(C═C)
825		827	γ(C–H) aromatic nuclei + $\delta(C \doteq C)$aromatic nuclei
869		876	β(C–H) aromatic nuclei
956	958	953	antiphase γ(C–H) aromatic nuclei
975	975	970	antiphase γ(C–H) QF, pure
997	996	997	γ(C–H) QF + γC-H (C═C)
1033	1029	1031	β(C–H) aromatic nuclei + βC-H (C═C)
1066		1067	β(C–H) QF + βC-H (C═C)
1170	1170	1170	β(C–H) aromatic nuclei + β(O–H)
1215		1217	β(C–H) aromatic nuclei + $\delta(CH_3)$
1286	1286	1283	βC-H (C]C) + δ(O–H)
1309	1309	1309	β(C–H) QF + βC-H (C]C) + ν(C–N)
1328	1326	1328	β(C–H) aromatic nuclei + βC-H (C═C)
1350		1351	βC-H (C═C) + β(C–H) NF + β(C–H) QF
1365	1365	1361	β(C–H) NF + β(C–H) QF + $\nu(C \doteq C)$aromatic nuclei
1404	1403	1406	β(C–H) C]C + $\nu(C \doteq C)$aromatic nuclei + ν(C–H) aromatic nuclei + δ^{s} (CH_3)
1469		1473	δ^{s} (CH_3)+ β(C–H) QF
1517		1519	δ^{s} (CH_3) QF + $\nu(C \doteq C)$ QF
1566	1563	1556	$\nu(C \doteq C)$ aromatic nuclei
1593	1590	1588	ν(C═C) + $\nu(C \doteq C)$aromatic nuclei

Abbreviations: BF – benzene fragment, QF quinoline fragment, ν - stretching vibration, δ - deformation vibration, β - in plane deformation vibration, γ - out of plane vibration.

(HSQC), and heteronuclear multiple-bond correlation spectroscopy (HMBC) methods. All spectra are included in the Supplementary data (Suppl. Figs. S10–S19). The signals of the CH-protons from the aromatic systems and the ethylene bridge can be seen in Fig. 11 in the range of 9.8 to 6.6 ppm.

It is instructive to trace the chemical shift of the protons along the charge transfer axis in the molecules of the two chromophores.

The reduced electron density (-M, –I of quinolinium N^+) of the 2-position proton in the quinolinium moiety is the reason why it gives a signal in the lowest field at 9.32 ppm for **D34** and 9.15 ppm for **D36.** Since H2 and H3 are vicinal, the doublet for the proton in the third position, H3, is detected at 8.45 ppm for **D34** and 8.35 ppm for **D36**. The two doublets for H2 and H3 protons in the spectrum of **D36** with $J = 6.7$ Hz are upfield shifted compared with the same signals in the **D34** spectrum. The chemical shifts of the protons from the bridging double bond much more adequately reflect the changes in the electronic structure of the dyes since they are distant from the ring current regions of the aromatic rings and the associated carbon atoms, therefore carrying the largest positive and negative charges. The signals for the two vinyl protons – H_α and H_β in the series of dyes synthesized by us generally appear in two variants: 1) as two doublets with a large J constant and with a difference in the chemical shift of the signals for these protons $\Delta\delta$(Hβ - Hα) up to around 0.6 ppm; 2) as the only singlet for two protons. The signals for these two protons appeared at 8.21 ppm and 8.02 ppm for Hβ and Hα in the **D36** spectrum, respectively. In the ^{1}H-NMR spectrum of the 4-hydroxy substituted dye **D34**, the signals for the ethenyl protons are part of a multiplet centered at 8.15 ppm, which contains two doublets with $J = 15.8$ Hz. These two protons are easily recognizable because of the high values of their spin-spin interaction constants in the 15–16 Hz interval, which is indicative of the *E (trans)*-configuration of the double bond. However, in the **D34** ^{13}C-NMR spectrum, the carbon atoms of the double bond are clearly discernible as signals at 144.37 (Cβ) and 116.38 (Cα), and 145.38 and 113.06 ppm for **D36**, respectively. In the benzene fragment of the dyes, four protons are present (two by two equivalent), which in ^{1}H-NMR appear as doublets at about 7.89 ppm (H2′ and 6′) and 6.9 ppm (H3′ and 5′), respectively.

Thus, due to the fact that the dyes **D34** and **D36** have different magnitudes of ICT interaction, this leads to a shifting of the proton resonance of the methine protons within Δδ 0.10–0.17 ppm between the same proton's signals. The same shifting in the ^{13}C-NMR spectra of both dyes is around 1.1–7.32 ppm.

4. Conclusions

Single-crystal X-ray diffraction studies of both dyes **D36** and **D34** clearly indicate that the cations in the crystals form face-to-face molecular pairs connected by π···π interactions. The results of the vibrational spectra of the dyes studied are in accordance with the X-ray structural study and show strong vibrational interaction between the aromatic nuclei by the ethylenic double bond, which is responsible for the interaction between them. On the basis of experimental measurements in a sufficiently wide range of solvents, we can conclude that both dyes show real reversible sovatochromic behaviour. The dye **D36** does not fluoresce, and **D34** shows very low emission in proton and aprotic dipolar solvents. Presumably in the **D36** molecule and to some extent in **D34**, the relaxation goes through a twisted intramolecular charge transfer (TICT) state, and this is the dominant non-radiative process.

The dyes displayed finely tuneable optical properties in the ground and excited states, which were dependent on the nature of substitution and solvent polarity.

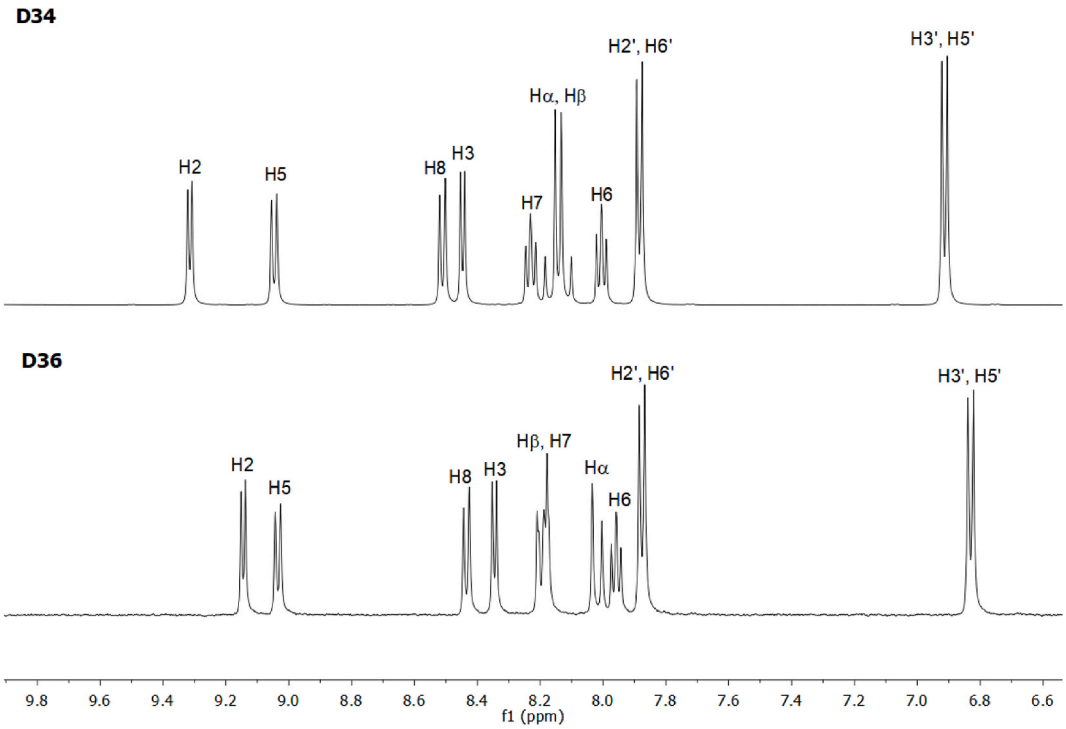

Fig. 11. Aromatic regions of the ^{1}H-NMR spectra of **D36** and **D34** in DMSO-d_6.

Data availability

CCDC 801043 contains the supplementary crystallographic data for this paper. The data can be obtained free of charge from the Cambridge Crystallographic Data Centre via www.ccdc.cam.ac.uk/structures.

CRediT authorship contribution statement

Mina Todorova: Writing – original draft, Validation, Investigation, Formal analysis, Data curation. **Rüdiger W. Seidel:** Writing – review & editing, Writing – original draft, Visualization, Validation, Resources, Investigation, Formal analysis, Data curation. **Mihaela Stoyanova:** Investigation. **Tsonko M. Kolev:** Writing – review & editing, Validation, Project administration, Methodology, Conceptualization. **Rumyana Bakalska:** Writing – review & editing, Writing – original draft, Visualization, Validation, Supervision, Resources, Project administration, Investigation, Formal analysis, Data curation, Conceptualization.

Declaration of competing interest

The authors declare that they have no known competing financial interests or personal relationships that could have appeared to influence the work reported in this paper.

Acknowledgements

This study is financed by the European Union-NextGenerationEU, through the National Recovery and Resilience Plan of the Republic of Bulgaria, project DUECOS BG-RRP-2.004-0001-C01.

We would like to thank Dr. Slava Tsoneva for measuring the IR/Raman spectra, Ivan Angelov for recording the fluorescence spectra and Dr. Richard Goddard for assistance with the Hirshfeld surface analysis. R.W.S. and T.M.K. are grateful to the late Professor William S. Sheldrick for his support of this research.

Appendix A. Supplementary data

Supplementary data to this article can be found online at https://doi.org/10.1016/j.heliyon.2024.e29315.

References

[1] M. Jazbinsek, A. Abina, A. Zidansek, Organic crystals for THz Photonics, Appl. Sci. 9 (5) (2019) 882–926, https://doi.org/10.3390/app9050882.
[2] P.N. Prasad, D.J. Williams, Nonlinear Optical Effects in Molecules and Polymers, Wiley, New York, NY, USA, 1991, 978-0-471-51562-3.
[3] R. Krieg, A. Eitner, W. Gunther, C. Schurer, J. Lindenau, K.-J. Halbhuber, N,N-Dialkylaminostyryl dyes: specific and highly fluorescent substrates of peroxidase and their application in histochemistry, J. Mol. Histol. 39 (2008) 169–191, https://doi.org/10.1007/s10735-007-9150-1.
[4] R. Krieg, A. Eitner, W. Gunther, K.-J. Halbhuber, Optimization of heterocyclic 4-hydroxystyryl derivatives for histological localization of endogenous and immunobound peroxidase activity, Biotec. Histochem. 82 (4–5) (2007) 235–262, https://doi.org/10.1080/10520290701714013.
[5] K. Senthil, S. Anand, S. Kalainathan, The effect of molecular structure on second-order nonlinear optical properties of stilbazolium derivative single crystals: a review, J. Mater. Chem. C 8 (2020) 16668–16690, https://doi.org/10.1039/D0TC04260A.
[6] H. El Ouazzani, S. Dabos–Seignon, D. Gindre, K. Iliopoulos, M. Todorova, R. Bakalska, P. Penchev, S. Sotirov, T. Kolev, V. Serbezov, A. Arbaoui, M. Bakasse, B. Sahraoui, Novel styrylquinolinium dye thin films deposited by pulsed laser deposition for nonlinear optical applications, J. Phys. Chem. C 116 (2012) 7144–7152, https://doi.org/10.1021/jp2118218.
[7] Cambridge Structural Database 1 January 2023 CSD Space Group Statistics – Space Group Frequency Ordering .https://www.ccdc.cam.ac.uk/media/CSD-Space-Group-Statistics-Space-Group-Frequency-Ordering-2023.pdf.
[8] R. Bakalska, M. Todorova, H. Sbirkova, B. Shivachev, T. Kolev, Comparing of the crystal structure and spectroscopic properties of some stilbazolium dyes with enlarged π-conjugated system I. Chromophores with p-dimethylamino group, Dyes Pigm. 136 (2017) 919–929, https://doi.org/10.1016/j.dyepig.2016.09.034.
[9] P. Antony, S. Bharanidharan, R.J. Vijay, S.J. Sundaram, P. Winston, J. A, L. Ligimolf, J. Jillyg, P. Sagayaraj, Structural, thermal, linear and nonlinear optical and cytotoxicity studies of a novel organic stilbazolium salt: 4-[2-(4-hydroxyphenyl)ethenyl]-1-methylpyridinium 4-styrenesulfonate, J. Mol. Struct. 1264 (2022) 133196, https://doi.org/10.1016/j.molstruc.2022.133196.
[10] K. Nivetha, W. Madhuri, S. Kalainathan, Synthesis, growth, crystal structure and characterization of new stilbazolium derivative single crystal: (E)-4-(3-ethoxy-2-hydroxystyryl)-1-methyl pyridinium iodide (3ETSI), J. Mater. Sci- Mater El., 28 (12) (2017) 8937–8949, https://doi.org/10.1007/s10854-017-6624-0.
[11] K. Nivetha, W. Madhuri, Structural, spectral, thermal, and optical studies of stilbazolium derivative crystal: (E)-4-(3-hydroxy-4-methoxystyryl)-1-methyl pyridinium iodide monohydrate, Opt. Laser Technol. 109 (2019) 496–503, https://doi.org/10.1016/j.optlastec.2018.08.035.
[12] X. Zhang, X. Jiang, Y. Li, Z. Lin, G. Zhang, Y. Wu, Synthesis, crystal structures and properties of new quinolinium derivatives, Chem. Phys. Lett. 641 (2015) 141, https://doi.org/10.1016/j.cplett.2015.10.062.
[13] T. Kolev, R. Bakalska, M. Todorova, M. Lamshoeft, H. Mayer-Figge, W.S. Sheldrick, B. Ivanova, M. Spiteller, Experimental Crystal Structure Determination, 2017, https://doi.org/10.5517/ccdc.csd.cc1q5fz9. CCDC 1584161.
[14] D. Schulte-Frohlinde, H. Güsten, Thermische cis-trans-Isomerisierung von 1-Äthyl-4-[4-hydroxy-styryl]-chinoliniumchlorids. Zur Existenz von cis-Stilbazoliumbetainen, Liebigs Ann. Chem. 749 (1971) 49–55, https://doi.org/10.1002/jlac.19717490107.
[15] S. Hünig, O. Rosenthal, Farbe und Konstitution II: Phenolbetainfarbstoffe, Liebigs Ann. Chem. 592 (1955) 161–177, https://doi.org/10.1002/jlac.19555920302.
[16] M.A. Clapp, R.S. Tipson, Studies in the quinoline series; some derivatives of 4-styrylquinoline, J. Am. Chem. Soc. 68 (1946) 1332–1334, https://doi.org/10.1021/ja01211a072.
[17] W. Schneider, A. Pothmann, Über die Lösungsfarben von Phenolbetainen der Chinolinreihe, Chem. Ber. 74 (1941) 471–493, https://doi.org/10.1002/cber.19410740402.

[18] a) I.N. Butnitskii, V.I. Voznyak, B.M. Gutsulyak, Lepidinium derivatives as growth and development regulators of plants. VI. p-(Dimethylamino) styrylquinolinium salts, Fiziologicheski Aktivnye Veshchestva 5 (1973) 108–110;
b) I.N. Butnitskii, V.I. Voznyak, B.M. Gutsulyak, Lepidinium derivatives as regulators of the growth and development of plants. VII. Relation between the chemical structure and physiological activity of some p-(dimethylamino)styrylquinolinium salts, Fiziologicheski Aktivnye Veshchestva 7 (1975) 62–64.
[19] V.I. Voznyak, L.G. Savitskaya, D.D. Neporadnyi, Antimicrobial activity of quaternary 4-(p-dimethylaminostyryl)quinolinium salts, Pharm. Chem. J. 18 (1984) 561–563, https://doi.org/10.1007/BF00779276.
[20] CrysAlisPro, Oxford Diffraction Ltd, Yarnton, Oxfordshire, England, 2009.
[21] R.H. Blessing, An empirical correction for absorption anisotropy, Acta Cryst. A51 (1995) 33–38, https://doi.org/10.1107/S0108767394005726.
[22] G.M. Sheldrick, A short history of SHELX, Acta Cryst. A64 (2008) 112–122, https://doi.org/10.1107/S0108767307043930.
[23] G.M. Sheldrick, Crystal structure refinement with SHELXL, Acta Cryst. C71 (2015) 3–8, https://doi.org/10.1107/S2053229614024218.
[24] P.R. Spackman, M.J. Turner, J.J. McKinnon, S.K. Wolff, D.J. Grimwood, D. Jayatilaka, M.A. Spackman, *CrystalExplorer*: a program for Hirshfeld surface analysis, visualization and quantitative analysis of molecular crystals, J. Appl. Crystallogr. 54 (3) (2021) 1006–1011, https://doi.org/10.1107/S1600576721002910.
[25] C.R. Groom, I.J. Bruno, M.P. Lightfoot, S.C. Ward, The Cambridge Structural Database, Acta Cryst. B72 (2016) 171–179, https://doi.org/10.1107/S2052520616003954.
[26] M.A. Spackman, D. Jayatilaka, Hirshfeld surface analysis, CrystEngComm 11 (2008) 19–32, https://doi.org/10.1039/B818330A.
[27] M.K. Kumar, S. Sudhahar, G. Bhagavannarayana, R. Mohan Kumar, Crystal growth, structural and optical properties of an organic ion-complex crystal: 4-N,N-dimethylamino-4′-N′-methylstilbazolium iodide, Optik 125 (2014) 5641–5646, https://doi.org/10.1016/j.ijleo.2014.05.046.
[28] I. Vijayakumar, J. Hubert, N.C.P. Reghunadhan, V.S. Jayakumar, Efficient π electrons delocalization in prospective push–pull non-linear optical chromophore 4-[N,N-dimethylamino]-4′-nitro stilbene (DANS): a vibrational spectroscopic study, Chem. Phys. 343 (2008) 83–99, https://doi.org/10.1016/j.chemphys.2007.10.033.
[29] J.-H. Jeong, J.-S. Kim, J. Campo, S.-H. Lee, W.-Y. Jeon, W. Wenseleers, M. Jazbinsek, H. Yun, O.-P. Kwon, *N*-Methylquinolinium derivatives for photonic applications: Enhancement of electron-withdrawing character beyond that of the widely-used N-methylpyridinium, Dyes Pigm. 113 (2015) 8–17, https://doi.org/10.1016/j.dyepig.2014.07.016.
[30] N.A. Murugan, J. Kongsted, Z. Rinkevicius, H. Agrena, Breakdown of the first hyperpolarizability/bond-length alternation parameter relationship, Proc. Natl. Acad. Sci. USA 107 (38) (2010) 16453–16458, https://doi.org/10.1073/pnas.1006572107.
[31] A. Teshome, M. Delower, H. Bhuiyan, G.J. Gainsford, M. Ashraf, I. Asselberghs, G.V.M. Williams, A.J. Kay, K. Clays, Synthesis, linear and quadratic nonlinear optical properties of ionic indoline and *N,N*-dimethylaniline based chromophores, Opt. Mater. 33 (2011) 336–345, https://doi.org/10.1016/j.optmat.2010.09.002.
[32] C. Reichardt, T. Welton, Solvents and Solvent Effects in Organic Chemistry, Wiley-VCH Verlag GmbH & Co. KGaA, 2011. Print ISBN:9783527324736.
[33] M. Todorova, R. Bakalska, T. Kolev, Synthesis, crystal structure, and spectroscopic properties of new stilbazolium salt with enlarged π-conjugated system, Spectrochim. Acta 108 (2013) 211–222, https://doi.org/10.1016/j.saa.2013.01.088.
[34] M. Dominguez, M.C. Rezende, Towards a unified view of the solvatochromism of phenolate betaine dyes, J. Phys. Org. Chem. 23 (2010) 156–170, https://doi.org/10.1002/poc.1599.
[35] M.C. Rezende, A generalized reversal model for the solvatochromism of merocyanines, J. Phys. Org. Chem. 29 (9) (2016) 460–467, https://doi.org/10.1002/poc.3565.
[36] A. Paudics, D. Hessz, M. Bojtár, B. Gyarmati, A. Szilágyi, M. Kállay, I. Bitter, M. Kubinyi, Binding modes of a phenylpyridinium styryl fluorescent dye with cucurbiturils molecules, Mol 25 (21) (2020) 5111–5126, https://doi.org/10.3390/molecules25215111.
[37] X. Cao, R.W. Tolbert, J.L. McHale, W.D. Edwards, Theoretical study of solvent effects on the intramolecular charge transfer of a hemicyanine dye, J. Phys. Chem. A. 102 (1998) 2739–2748, https://doi.org/10.1021/jp972190e.
[38] Y. Huang, T. Cheng, F. Li, C. Luo, C.-H. Huang, Z. Cai, X. Zeng, J. Zhou, Photophysical studies on the mono- and dichromophoric hemicyanine dyes II. Solvent effects and dynamic fluorescence spectra study in chloroform and in LB films, J. Phys. Chem. B 106 (2002) 10031–10040, https://doi.org/10.1021/jp020877f.
[39] B. Strehmel, H. Seifert, W. Rettig, Photophysical properties of fluorescence Probes. 2. A model of multiple fluorescence for stilbazolium dyes studied by global analysis and quantum chemical calculations, J. Phys. Chem. B 101 (1997) 2232–2243, https://doi.org/10.1021/jp962835v.
[40] B. Ivanova, T. Kolev, Linearly polarized IR spectroscopy: theory and applications for structural analysis, chapter 1, in: Effects in the Infrared Spectra of Crystals, CRC Press, Taylor & Francis Group, Boca Raton, London, New York, 2012, pp. 23–27, 978-1-4398-2559-4.
[41] M. Todorova, R. Bakalska, Syntheses and vibrational spectroscopic characteristics of series ionic merocyanine dyes, Bulg. Chem. Commun. 50 (J) (2018) 156–164.